THE ASTROPHYSICAL JOURNAL, 330:399–414, 1988 July 1

MOLECULAR CLOUDS IN THE OUTER GALAXY. III. CO STUDIES OF INDIVIDUAL CLOUDS

KATHRYN N. MEAD[1]
Physics Department, Rensselaer Polytechnic Institute, and E. O. Hulburt Center for Space Research, Naval Research Laboratory

AND

MARC L. KUTNER
Physics Department, Rensselaer Polytechnic Institute
Received 1987 April 8; accepted 1987 December 1

ABSTRACT

Physical conditions and related star-forming activities have been investigated in 31 molecular clouds in the outer Galaxy. All clouds were mapped in the CO ($J = 1 \rightarrow 0$) line. In addition, overlapping subsets of 10 clouds were mapped in ^{13}CO ($J = 1 \rightarrow 0$) and 11 in CO ($J = 2 \rightarrow 1$). On a large scale, the clouds follow the H I warp, and there appears to be an arm at $R \sim 13$ kpc, coincident with a feature in the H I surface density distribution. Studying individual clouds reveals the following results. (1) Peak T_R*'s are found to decrease somewhat with distance, d, indicating that the peaks are beam diluted. Typical peak T_R*'s are a few K, the largest is 10 K. (2) Qualitative analyses of the CO ($J = 1 \rightarrow 0$ and $J = 2 \rightarrow 1$) line strengths in the cloud envelopes indicate low kinetic temperatures (T_k) in the clouds. Computer models confirm that, in the envelopes, a T_k of 7 K can produce the line strengths observed in the three species. Models run with larger (10 and 13 K) kinetic temperatures produce greater line strengths than observed, especially in the ^{13}CO line. (3) Line strength ratios of the CO ($J = 1 \rightarrow 0$) and ^{13}CO ($J = 1 \rightarrow 0$) lines at and near the cloud peaks are typically between 3 and 6, indicating that the CO line is optically thick. (4) Most clouds lie between $R = 11.5$ kpc and $R = 14$ kpc. At larger Rs few clouds were found and they have drastically lower line strengths, indicating that the CO at $R > 14.5$ kpc is either sparse or cold. (5) An average cloud is 40 pc in the longest dimension. (6) Most observed clouds have masses in the range 10^4–10^5 $M_\odot$.

Subject headings: galaxies: The Galaxy — interstellar: molecules

I. INTRODUCTION

The outer Galaxy provides an opportunity to study molecular clouds and star formation in a different environment from the inner Galaxy. These differences are discussed by Mead *et al.* (1987, hereafter Paper I). In assessing the effects of these environmental factors, we must first determine how the basic characteristics (e.g., size and mass distributions, temperature, and density) of outer Galaxy clouds differ from those of inner Galaxy clouds. In this paper, we present an analysis of 31 outer Galaxy clouds, chosen from an undersampled CO survey of a piece of the outer Galaxy (Kutner and Mead 1981, hereafter KM). CO spectra and contour maps for these 31 clouds appear in Mead (1987, hereafter Paper II).

KM roughly estimated of the mass of H_2 in the outer Galaxy to be $\sim 3 \times 10^8$ $M_\odot$. Based on a more completely sampled survey of a small region in l, but 4° in b, Kutner and Mead (1985) estimated the mass to be $\sim 5 \times 10^8$ $M_\odot$ (the spectra appear in Kutner 1983 and Mead 1986*b*). For comparison, Solomon, Stark, and Sanders (1983) find the mass to be $\sim 2 \times 10^8$ $M_\odot$, using essentially the same conversion factor from CO luminosity to H_2 mass as was used by Kutner and Mead (1985). We attribute most of the factor of ~ 2 discrepancy to the fact that Solomon *et al.* (1987) assumed a scale height, while Kutner and Mead (1985) measured the z-distribution. At this point, the largest uncertainty about the mass of H_2 in the outer Galaxy results from the lack of sufficient (l, b) coverage in any of the existing surveys.

A comparison of inner and outer Galaxy H I and H_2 masses points out another important aspect of studies of the outer Galaxy. Estimates of the mass of H_2 inside the solar circle fall in the range ~ 1–2×10^9 $M_\odot$. Henderson, Jackson, and Kerr (1982, hereafter HJK) find the mass of H I to be $\sim 1 \times 10^9$ $M_\odot$ inside the solar circle and $\sim 2 \times 10^9$ $M_\odot$ outside the solar circle (using $R_0 = 10$ kpc). This means that inside the solar circle, roughly half of the interstellar medium is molecular, with that fraction being higher at the peak of the "molecular ring." In the outer Galaxy, the H_2 is about 20% of the interstellar medium. This minority role is typical for a number of galaxies that still have consequential massive star formation. It may therefore be that in comparing star formation in the inner and outer Galaxy we may learn more about star formation under the broad range of conditions that exist in other galaxies.

Star formation in the outer Galaxy is the subject of Paper I in which 50 and 100 μm data taken from the Kuiper Airborne Observatory were presented and discussed along with 6 cm continuum data taken with the VLA. This study has since been expanded to include *IRAS* data and 6 and 20 cm VLA data on 17 outer Galaxy clouds (Mead, Kutner, and Evans 1988; Paper IV). Calculated spectral types of the illuminating stars range from B3 to O5.

II. OBSERVATIONS

Observations of CO ($J = 1 \rightarrow 0$) ($\lambda = 2.6$ mm) were made in 1981 June and November and 1982 February with the NRAO[2]

[1] National Research Council/NRL Cooperative Research associate.

[2] The National Radio Astronomy Observatory is operated by Associated Universities, Inc., under contract with the National Science Foundation.

11 m telescope, on Kitt Peak. The half-power beam width was 70″. After the telescope was equipped with a more accurate 12 m surface, observations of ^{12}CO ($J = 2 \rightarrow 1$) ($\lambda = 1.3$ mm) were made in 1985 January. A complete description of all the observations appears in Mead (1988; Paper II).

The intensities are expressed as T_R^*, the antenna temperature corrected for atmospheric attenuation, ohmic losses, and rear and forward spillover (Kutner and Ulich 1981). The forward spillover and scattering efficiency, η_{fss}, was 0.74 at 2.6 mm and 0.8 at 1.3 mm (P. Jewell, private communication). Radiation temperatures, T_R, can be obtained from the expression T_R^*/η_c, where η_c is the source coupling efficiency. For sources 1′ to a few arcminutes in extent $\eta_c \approx 0.8$ at 2.6 mm (Kutner, Mundy, and Howard 1984) and at 1.3 mm (P. Jewell, private communication). At 2.6 mm absolute values of T_R^* should be accurate to within 10%. At 1.3 mm absolute values of T_R^* should be good to 20% and relative T_R^*'s should be good to 10%. Typical rms noise levels for the $1 \rightarrow 0$ spectra are 0.3 K; for the $2 \rightarrow 1$ spectra: 0.2 to 0.3 K; and for the ^{13}CO spectra: 0.08 to 0.1 K.

III. RESULTS

All of the spectra and contour maps appear in Paper II. Table 1 contains observed line parameters for all clouds in which CO was detected. The "Name" (col. [1]) is an approximate Galactic longitude and latitude for each cloud; it corresponds to the position on a 0.1 × 0.1 grid where the cloud was first detected, so it does not necessarily correspond to any peak in the cloud. Generally, at least one line peaks at the position given in a row. In column (2) is listed the data class, a number indicating the relative quality of the data (see below). Following the 1950.0 coordinates are the distance from the Galactic center, R, and the distance from the Sun, d. These are kinematic distances, based on a flat rotation curve, with $R_0 = 8.5$ kpc and $v_0 = 220$ km s^{-1}. The line parameters $I (= \int T_R^* dv)$, T_R^*, and v for each species are given in the following nine columns. If a cloud was not observed in a given species, the species column is blank at the rows for that cloud. If a cloud was observed in a species but a particular position was not observed, the phrase "not observed" appears in that cell. The column labeled "Peak" indicates the importance of a tabulated position. A maximum in integrated intensity or T_R^* is indicated by an I or a T, respectively, followed by a code for the species; 12, 13, or 21 for ^{12}CO, ^{13}CO, and CO ($J = 2 \rightarrow 1$), respectively. So, for example, $I21$ in a column means that the largest CO ($J = 2 \rightarrow 1$) integrated intensity was observed at that position. Peaks at the cloud velocity are listed first, peaks of other velocity components are listed second. If a second velocity component constitutes a separate cloud it is listed separately and indicated by a repetition of the name.

There are 31 clouds in the table including the five clouds from Kutner and Mead (1981) (identified by the data class designation KM). These clouds are divided into two groups by the quality of the data. (1) Clouds whose data are of good or better quality number 23. The five KM clouds have data of this quality but they are denoted separately in the figures and tables. (2) There are three cases of clouds with few lines or a low signal-to-noise ratio. There is no uncertainty as to the detection of these clouds; they are segregated only because the observed and derived quantities are not as accurate as those in the first group. We have also detected three clouds which have $|v_{1sr}| \geq 90$ km s^{-1}, putting them at the largest Rs in the survey. Several possible high-velocity clouds (large d and R) were observed in order to examine the extent (in R) of molecular emission. These distant clouds are discussed further in Mead (1986*b*).

a) Galactic Distribution of Clouds

Kinematic distances to all clouds and velocity components have been derived assuming $R_\odot = 8.5$ kpc and $v_\odot = 220$ km s^{-1} and a flat rotation curve. Though Brandt's rotation curve (1986) is more realistic, it is nearly flat so the latter was chosen for simplicity. Table 2 lists the distance, d, the galactocentric distance, R, the height above the Galactic plane, z, and the number of parsecs per arcminute at the kinematic distance.

To give the reader an idea of the location of the clouds in the Galaxy, they are plotted (using kinematic distances) as they would appear in an overhead view of the Galaxy in Figure 1. The clouds lie in a band centered at roughly $R = 13$ kpc. For comparison of the overall distribution of the CO clouds and the H I surface density, a plot of the latter (taken from *HJK*) is shown in Figure 2. (Fig. 2 is drawn using the "old" Galactic constants, as noted in the figure.) The surface density feature evident in Figure 2 is sometimes referred to as the "outer arm." Of course, to properly establish the existence of a molecular arm, a fully sampled survey of reasonable l and v coverage must be done. However, given the present evidence we expect that such a study would reveal a well-defined molecular arm in the outer Galaxy (beyond the Perseus arm). In the next two paragraphs we address problems of deriving $l - R$ information from $l - v$ information and of interpreting our data as evidence for an arm.

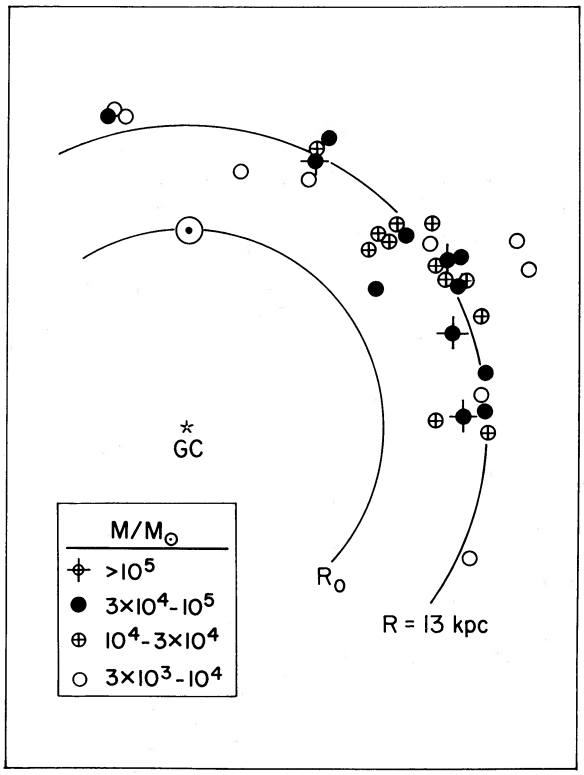

FIG. 1.—Positions of clouds are plotted as function of R and z in this overhead view of the galaxy. For $R > R_0$ a flat rotation curve was assumed, and the galactic constants $R_0 = 8.5$ kpc and $v_0 = 220$ km s^{-1} were used. The line at $R = 13$ kpc is for reference.

TABLE 1

CARBON MONOXIDE PEAKS

Name	Data Class	R. A. (1950)	Dec.	R^a (kpc)	d^a (kpc)	$^{12}CO(J=1-0)$			$^{13}CO(J=1-0)$			$^{12}CO(J=2-1)$			Peak	Notes
						I^b	T^c	v^d	I^b	T^c	v^d	I^b	T^c	v^d		
(1)	(2)	(3)	(4)	(5)	(6)	(7)	(8)	(9)	(10)	(11)	(12)	(13)	(14)	(15)	(16)	(17)
G52.7+1.5	2	19 20 53.8	18 10 57.7	10.7	13.4	15.2	1.7	-58.7							I12 T12	
		19 20 49.5	18 9 57.8			6.6	3.0	-36.6							T12	
		53.8				7.7	2.7	-37.2							I12	
G56.7+1.3	2	19 30 1.9	21 32 35.	13.0	15.6	11.6	1.3	-67.7							I12 T12	1
G56.8+1.9	1	19 27 41.6	21 53 16.3	12.0	14.4	18.0	3.2	-54.2	not observed						I12	
		28.7	51 16.7			9.8	3.6	-54.9	0.6	0.5	-54.4				T12	
		50.2	48 16.5			not observed			2.8	0.9	-57.1				I13 T13	
G59.9+1.5	KM	19 36 00.9	24 24 49.0	12.9	14.9		3.3	-65.0							T12	
		52.1														
G62.2+1.7	1	19 40 9.6	26 31 30.1	12.9	14.4	9.6	3.3	-66.6				12.4	4.2	-67.0	I12 T12	2
			32 00.									22.2	7.2	-67.0	I21 T21	3
			30.1			5.1	1.8	-67.9				11.4	4.4	-67.6	.5'N of I21 T21	4
G65.5+1.3	KM	19 49 21.8	29 09 57.0	13.1	14.1		3.5	-71.0							T12	
G69.7+1.5	KM	19 59 03.0	32 54 01.0	13.2	14.2		4.8	-63.0							T12	
G74.1+1.5	1	20 10 5.5	36 33 46.5	10.2	8.4	17.6	3.8	-36.2				10.5	2.8	-36.2	I12 T12	
		8.0	33 46.9									12.9	3.1	-36.9	I21 T21	
		20 10 10.5	36 26 46.5			7.2	2.1	-57.0				not observed			T12	
		20.4	32 46.6			9.9	1.6	-59.0				not observed			I12	
G75.0+1.9	1	20 11 27.9	37 31 29.7	13.6	13.1							10.1	3.8	-81.6	T21	
			32 00.0									11.2	2.9	-81.0	I21	
		30.3				7.5	1.6	-81.6								5
		25.3				14.0	2.3	-79.0								6
		20.2	31 0.3			17.3	3.0	-77.1							I12 T12	
G78.8+1.7	1	20 23 4.6	40 29 50.3	13.1	11.8	33.7	7.0	-76.0	5.7	2.0	-76.0	29.9	5.7	-77.3	I12 T12 T13	7
		22 56.6				9.7	3.5	-76.0	8.9	1.6	-76.0	5.8	1.7	-76.6	I13	8
		59.3	49.6									8.1	3.3	-76.0		9
		23 4.5	30 19.7									31.3	7.6	-75.3	I21 T21	
G80.1+1.9	1	20 26 14.4	41 43 8.5	12.8	11.2	12.9	3.7	-72.1				12.8	3.8	-73.0	I12 T12 I21 T21	10
G80.4+1.9	2	20 27 13.9	41 52 41.4	13.5	12.0	11.3	1.1	-81.4							I12 T12	
G83.3+1.9	1	20 36 51.1	44 16 20.3	12.8	10.6	7.6	2.8	-73.4							T12	
		45.6	11 50.6			16.0	1.3	-71.4							I12	
		34.4				8.9	1.7	-72.1							2nd I12	

TABLE 1—*Continued*

Name	Data Class	R. A. (1950)	Dec.	R[a] (kpc)	d[a] (kpc)	^{12}CO(J=1-0) I[b]	^{12}CO(J=1-0) T[c]	^{12}CO(J=1-0) v[d]	^{13}CO(J=1-0) I[b]	^{13}CO(J=1-0) T[c]	^{13}CO(J=1-0) v[d]	^{12}CO(J=2-1) I[b]	^{12}CO(J=2-1) T[c]	^{12}CO(J=2-1) v[d]	Peak	Notes
(1)	(2)	(3)	(4)	(5)	(6)	(7)	(8)	(9)	(10)	(11)	(12)	(13)	(14)	(15)	(16)	(17)
G84.7+1.9	1	20 42 17.1	45 18 58.	13.6	11.4	33.6	6.2	-82.9							I12	
			19 57.9			31.8	7.1	-83.6							T12	
G84.7+1.7	KM	20 42 19.2	45 20 29	13.6	11.4		7.0	-83.0							T12	
G85.0+2.4	1	20 40 37.9	45 55 40.4	11.0	7.8	29.7	10.0	-51.0							I12 T12	
G85.0+2.4	1	20 40 37.9	45 53 40.5	13.7	11.5	12.8	3.4	-82.8							I12	
		43.6				11.2	3.5	-82.8							T13	
G88.4+1.9	1	20 55 12.2	48 16 52.7	11.9	8.6	13.0	1.6	-65.3	not observed			not observed			I12	
		54 24.0	9 53.0			6.7	3.2	-63.4	not observed			not observed			T12	
		55 12.2	12 52.9			7.7	3.0	-62.7	2.3	0.9	-63.3	not observed			I13	11
			13			8.4	2.9	63.3	1.6	1.0	-62.6	not observed			T13	
		18.3	13 52.9									7.3	2.6	-63.2	I21	
		33.2										5.7	2.9	-63.8	T21	
G88.4+1.9	1	20 55 30.2	48 12 52.9	13.3	10.4	6.7	1.9	-79.6	not observed			3.0	1.8	-79.4	I12	
		36.2	13 52.8			4.9	2.7	-79.0	not observed			5.7	2.5	-79.4	T12	
		55 30.1				4.2	2.2	-79.0	1.3	0.5	-78.9	6.9	2.5	-79.4	I13 T13	
		33.2	14 22.8									5.5	2.8	-79.4	T21	
		30.2	13 22.9									6.9	2.8	-79.4	I21 T21	
G88.8+1.9	1	20 56 40.9	48 21 0.	11.8	8.3	9.1	4.0	-60.6	2.2	1.4	-60.3	14.9	5.5	-60.7	I12 T12 I13 T13	
		43.9										20.2	7.6	-60.7	I21 T21	
		20 56 34.8	48 27 00.0			3.4	1.8	-83.3	not observed						T12	
		46.9	25			4.7	1.1	-79.4	not observed						I12 2ndT12	
		20 56 46.8	48 21 00.0						0.9	0.3	-76.0					12
G89.9+1.3	KM	20 59 52.7	48 42 30	12.6	9.2		7.3	-71.0							T12	
G92.9+1.9	1	21 14 30.1	51 34 46.2	13.8	10.4	16.0	3.2	-87.7							I12	13
		33.4										3.6	2.0	-87.6	3s E of I12	
												3.6	1.4	-82.4	3s E of I12	
		42.9				13.8	4.1	-87.1				8.8	3.2	-87.6	T12	
												4.3	2.2	-82.4	T12	
		13.9	33 15.8			not observed						22.8	4.9	-86.9	I21 T21	
		4.2	34 46.9						2.9	0.9	-80.1				T13	
			32 46.9			2.5	1.3	-85.8	3.5	0.6	-82.2				I13	
G93.2+1.7	1	21 16 39.8	51 39 11.0	12.7	9.0	21.2	5.8	-71.0	not observed						I12	14
			38 11.1			16.6	6.1	-71.0	not observed						T12	
		33.3	11.4			8.4	3.3	-71.6	5.8	1.1	-71.0				I13 T13	

TABLE 1—*Continued*

Name	Data Class	R. A. (1950)	Dec.	R[a] (kpc)	d[a] (kpc)	^{12}CO(J=1-0) I[b]	T[c]	v[d]	^{13}CO(J=1-0) I[b]	T[c]	v[d]	^{12}CO(J=2-1) I[b]	T[c]	v[d]	Peak	Notes
(1)	(2)	(3)	(4)	(5)	(6)	(7)	(8)	(9)	(10)	(11)	(12)	(13)	(14)	(15)	(16)	(17)
		21 16 20.5	51 35 10.9	11.3	6.9	5.2	1.8	-54.7							I12 T12	
		59.2	36 10.9			5.2	1.6	-54.7							I12	
G115.2+2.0	1	23 38 0.	63 35 27.6	12.0	5.6	12.8	4.7	-58.0							I12 T12	15
G120.8+1.1	1	00 29 10.8	63 38 54.9	12.9	6.2	30.3		-63.7	3.2	1.1	-63.7				I12 I13 T13	16
		47.1	41 54.8				4.0		not observed						T12	17
G123.5+2.0	1	00 54 17.0	64 29 43.1	13.2	6.4	11.1	1.8	-66.4				5.1	1.0	-62.4	I12 T12 I21 T21	18
G124.4+2.0	1	1 1 33.9	64 38 51.6	14.0	7.3	19.8	3.3	-72.3	not observed			not observed			I12	
		15.2				13.9	3.4	-72.3	not observed			not observed			T12	
		2 20.8	25 52.0			6.2	1.8	70.4	3.8	1.3	-71.0	not observed			I13 T13	
		2.1	28 51.9									6.4	2.6	-71.7	I21 T21	
G140.5+0.5	1	3 9 50.8	58 17 19.4	11.3	3.4	24.9	6.6	-37.3							I12	19
		35.5	19 19.3			19.0	7.2	-38.6							T12	
G211.4-1.1	1	6 42 12.8	0 55 49.5	13.6	5.6	8.3	3.4	44.9	not observed						I12 T12	20
G212.1-1.1	1	6 43 34.2	0 26 33.2	13.8	5.9	21.5	2.2	43.7	not observed						I12	
		26.2	0 16 33.4			14.7	5.4	45.0	not observed						T12	21
		22.2	20 32.9			6.4	1.5	41.8	2.5	0.5	42.3				I13	
		26.2				9.6	3.1	44.4	1.4	0.8	44.3				T13	
G215.0+0.9	1	6 56 0.7	-1 25 39.7	13.7	5.9	44.2	3.5	49.2				7.2	2.2		I12 T12	
		2.7										10.6	2.2	47.7	I21 T21	
			26 39.7									10.1	2.2	48.3	T21	

[a] Kinematic parameters were calculated using a flat rotation curve with $R_\odot = 8.5$ kpc and $v_\odot = 220$ km s^{-1}.

[b] $I = \Sigma T_R^* \delta v$(K km s^{-1}), where δv is the channel width.

[c] $T = T_R^*$ (K).

[d] $v = v_{LSR}$ (km s^{-1}).

NOTES.—(1) There is evidence for another velocity component at −85 km s^{-1}. (2) *I*12 position is 0.5 S of *I*21. (3) *I*21 position is 0.5 N of *I*12. (4) This position is 0.5 N of *I*21. (5) 0.5 E of *I*21. (6) 0.5 W of *I*21. (7) 2–1 position is at 49.″7. (8) 2–1 position is at 49.″7. (9) 4″E of *I*13. (10) 2–1 position is at 7.″9. (11) ^{12}CO(1–0) position is at 53.″2. (12) This is the only ^{13}CO line at −76 km s^{-1}. (13) Integrated intensities are the sum of two blended velocity components at −82 and −87 km s^{-1}. The two lines can be seen most clearly in the 2–1 spectra (see Mead 1988). (14) There is another velocity component at −55 km s^{-1}. (15) There are three lines at −71 km s^{-1} at (T_R^* =) 1 K in this cloud. (16) Only two positions were observed in ^{13}CO. (17) The ^{13}CO position is at 55.″6. (18) Only four positions were observed in 2–1, with two detections. (19) There is another cloud at −70 km s^{-1} in this direction. (20) Four positions were observed in ^{13}CO. (21) There are three lines at 51 km s^{-1} stronger than 1 K (T_R^*) in this direction.

TABLE 2

CLOUD ENVELOPE TEMPERATURES

Cloud	T_R*(1–0)	T_R*(2–1)
G74.1+1.5	2.2	3.0
G75.0+1.9	1.6	2.0
G78.8+1.7	1.5	2.8
G88.4+1.9 $v = -63$	1.8	2.5
$v = -79$	1.8	3.0
G92.9+1.9	2.0	2.5
G123.5+2.0	0.8	1.5
G124.4+2.0	1.5	2.5
G215.0+0.9	1.3	2.0
Average T_R*	1.6	2.4
Average T_R	2.0	3.0

Some of the uncertainties in kinematic distances that could create an "artificial arm" are as follows. (1) Use of the wrong rotation curve will systematically shift the clouds to incorrect Rs. This may distort an arm, but will not sweep randomly distributed clouds into an armlike feature. (2) Random deviations (due to clouds' velocity dispersion) from circular velocities will introduce random errors to kinematic distances. This might make an arm appear wider, but cannot create an artificial arm. (3) Streaming motions will introduce systematic errors into the kinematic distances (Burton 1972). As pointed out by Kulkarni, Blitz, and Heiles (1982), a more extensive analysis of the velocity field in the outer Galaxy is needed before the point is definitively settled. However, if streaming motions are important in this regard, their effects should be minimized where $|dv_r/dR|$ is relatively large. This is the case for the (l, v, R) range of the possible arm discussed in this section (where $|dv_r/dr| > 10$ km s^{-1} kpc^{-1}).

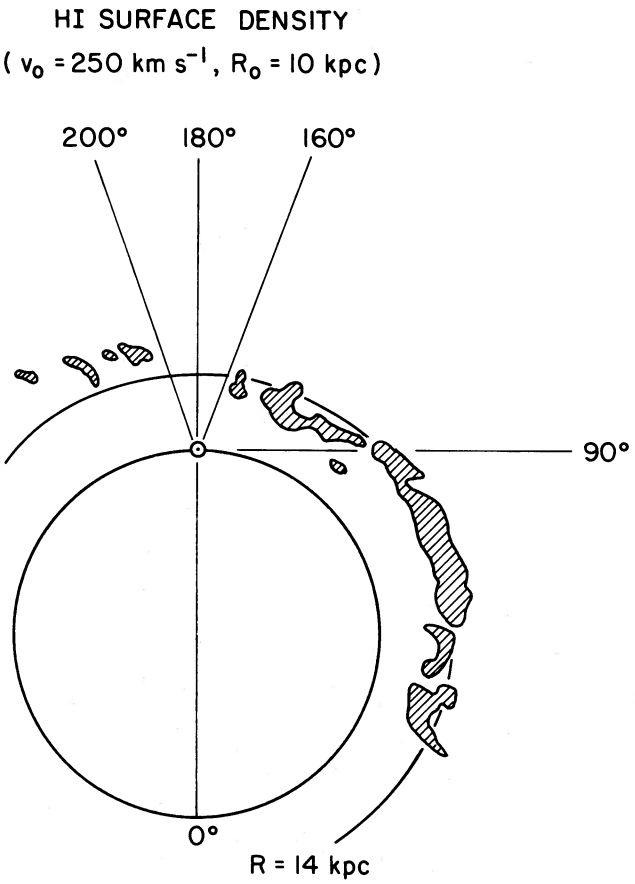

FIG. 2.—Plot of the H I surface density (from Henderson, Jackson, and Kerr 1982) is shown for comparison to the distribution of molecular clouds. Notice that the "old" Galactic constants were used in this figure.

The bias in our sample could produce an armlike feature, such as that seen in Figure 1. Consider the following. (1) We chose for mapping clouds that were clearly outside the solar circle and (2) lines from clouds beyond $R = 14$ kpc are weak (see § IV*a*). Therefore, the observed clouds with the best data lie in a band between about 10 and 14 kpc from the Galactic center. If data are taken in an armlike band, the results will look like an arm. However, the counterargument to this is that an arm is likely to be ~ 1 kpc wide, plus the effects of random cloud motions. Except for a few of the less massive clouds, the clouds in Figure 1 lie in a band ~ 2 kpc wide. Furthermore, the region between the solar circle and $R = 11.5$ kpc is relatively unpopulated with clouds. Since clouds in this region are easier to see (due to their larger angular extent), the contrast between this region and the region between 12 and 14 kpc seems even more striking as evidence for an arm-interarm contrast. (This contrast is even more evident in the uniformly sampled grid from $l = 85°$ to 85°.7 and $b = 0°$ to 4°, discussed by Kutner [1983; 1985] and Mead [1986*b*].)

We next consider the z-distribution of the clouds. Figure 3 is an outward-looking view of the Galaxy; clouds' positions are plotted as a function of l and z. The clouds follow the warp evidenced in H I. In particular, the molecular clouds follow the peak intensity of H I, which is farther from the plane than the centroid of H I emission.

Molecular clouds do lie in the H I warp. But since the clouds were chosen from a survey which was confined to the warp it is natural to ask whether there are clouds outside the warp as well. From the grid mentioned above, it was found that CO emission was seen around $b = 2°$ but not at the top and bottom of the grid, $b = 0°$ and $b = 4°$, indicating that the extent of the CO emission had been observed. In our survey, generally little emission was seen at the b limits of the observed strips. Further evidence that the CO emission does not extend beyond the H I warp is provided by Clemens *et al.* (1986) who have done a fully sampled survey of CO ($J = 1 \rightarrow 0$) near the plane, $|b| < 1°$. They report "very little emission at negative velocities and $l > 52°$ [in the first quadrant]" indicating that only a small amount of outer Galaxy CO is present near the plane.

b) Observed Quantities for Individual Clouds

To illustrate what typical line parameters are in outer Galaxy clouds, histograms of maximum and average ^{12}CO ($J = 1 \rightarrow 0$) line parameters (T_R*, $\Delta v = I$/peak T_R*, $I = \int T_R^* dv$) are shown in Figure 4, with clouds grouped by data class. (Averages are of individual spectra of positions with lines. No correction for incomplete sampling was made.) Data class 2 clouds populate lower T_R* bins and higher Δv bins than average data class 1 clouds because class 2 clouds are characterized by weak lines, and therefore baseline curvature has more of an effect on the line parameters (weak lines may be narrower than they appear).

Most peak T_R*'s are between 3 and 4 K. The largest peak T_R* is 10 K. It is notable that these temperatures are lower than those in the peaks of well-studied inner Galaxy giant

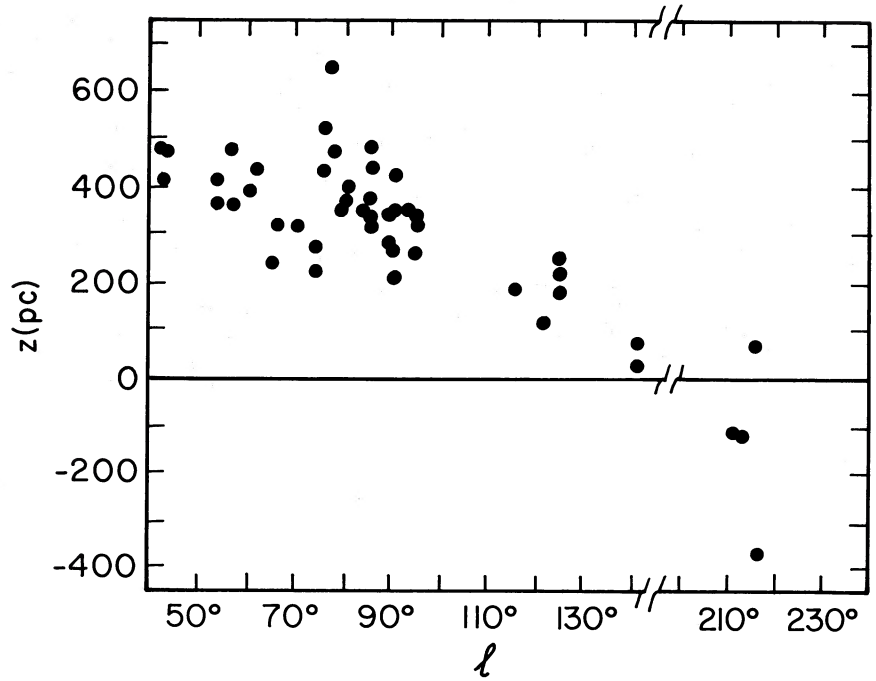

FIG. 3.—Cloud height above the Galactic plane, z, as a funtion of l in this outward-looking view of the Galaxy

molecular clouds (GMCs). Possible explanations for this will be discussed in § IV.

One cloud has an average T_R^* of 3.6 K, all others have average T_R^*'s of 3 K or less. No data class 1 clouds have average T_R^*'s less than 1 K. Because most lines are in the cloud envelope, an average quantity is slightly larger than the value of that quantity in the envelope. (For these clouds the cloud's molecular peak is generally less than a beamwidth in extent, two to three beamwidths in a few cases. Therefore, "envelope" generally refers to all positions in the cloud except the one or two strongest positions.) Inspection of the spectra maps shows that most non peak positions have T_R^*'s between 1 and 2 K, confirming that the cloud envelope line strengths are in the 1 to 2 K range. These temperatures seem low compared to envelopes of inner Galaxy and local clouds.

IV. DISCUSSION

a) Distance Effects on T_R^*

It is important to address the effect of beam dilution on our results for (at least) two reasons. (1) If our sources are beam diluted, it makes the conversion of observed quantities (e.g., T_R^*) to derived quantities (e.g., peak kinetic temperature) more difficult and uncertain. (2) Beam diluted emission may remain undetected without sufficient sensitivity. It should be remembered that both peaks *and* clumpy envelopes can be beam diluted. The latter situation is more difficult to recognize because it depends on a filling factor which could be independent of cloud distance. The most that we might be able to deduce is whether that filling factor varies with R. In the following analysis our primary goal will be to appraise if, and how much, beam dilution of the peaks is affecting our results. Using the kinematic distances, T_R^* versus R and T_R^* versus d are plotted to see if the line strengths systematically weaken with galactocentric or heliocentric distance.

In the case of outer Galaxy clouds, distance can affect antenna temperature in two ways, one instrumental and one real. (1) The peak may be beam diluted. If this occurs, it must be remembered that the material surrounding the diluted peak does produce some emission which is detected. Therefore, the observed T_R^* will not fall off simply as $1/d^2$. We have simulated this effect, using CO maps of real local GMCs with warm cores. At $d = 5$ kpc, the observed T_R^* is typically 75% of its value for the same cloud at 1 kpc; by $d = 10$ kpc, the falloff is only an additional 5%, and, by $d = 20$ kpc, an additional 10%. We would therefore not expect a dramatic falloff in T_R^* versus d, for the range of d in our study, even if beam dilution is significant. (2) If the frequency of embedded high-mass stars varies with R, then (assuming the gas is heated by the embedded stars) the peak CO temperatures should also vary with R (and therefore with d, since it is a function of R). In addition to the initial mass function, the coupling between the energy of the stars and molecular cloud may also vary with R, due to varying physical conditions (density, metallicity, velocity structure, etc.).

In an effort to investigate these effects, we have plotted peak and average T_R^* versus R in Figure 5, and versus d in Figure 6. (We note that when we chose clouds from the survey to be mapped, low T_R^* clouds at R close to R_0 were not considered as interesting as low T_R^* clouds at large R, as any cloud at larger R is interesting. So the paucity of clouds with low T_R^*'s at smaller Rs is probably a selection effect.)

The most striking feature of Figure 5 is the absence of clouds beyond $R \sim 14$ kpc. (There are low-luminosity clouds out to $R = 20$ kpc; Mead 1986*b*. See also Brandt 1986.) This may be the result of a smooth falloff in CO luminosity with R. It is more likely, though, that this figure illustrates the demarcation between a 13 kpc arm and an interarm region beyond it. Carbon monoxide emission has been detected from (what may be) cool "interarm" clouds beyond 14 kpc (Mead 1986*b*). To

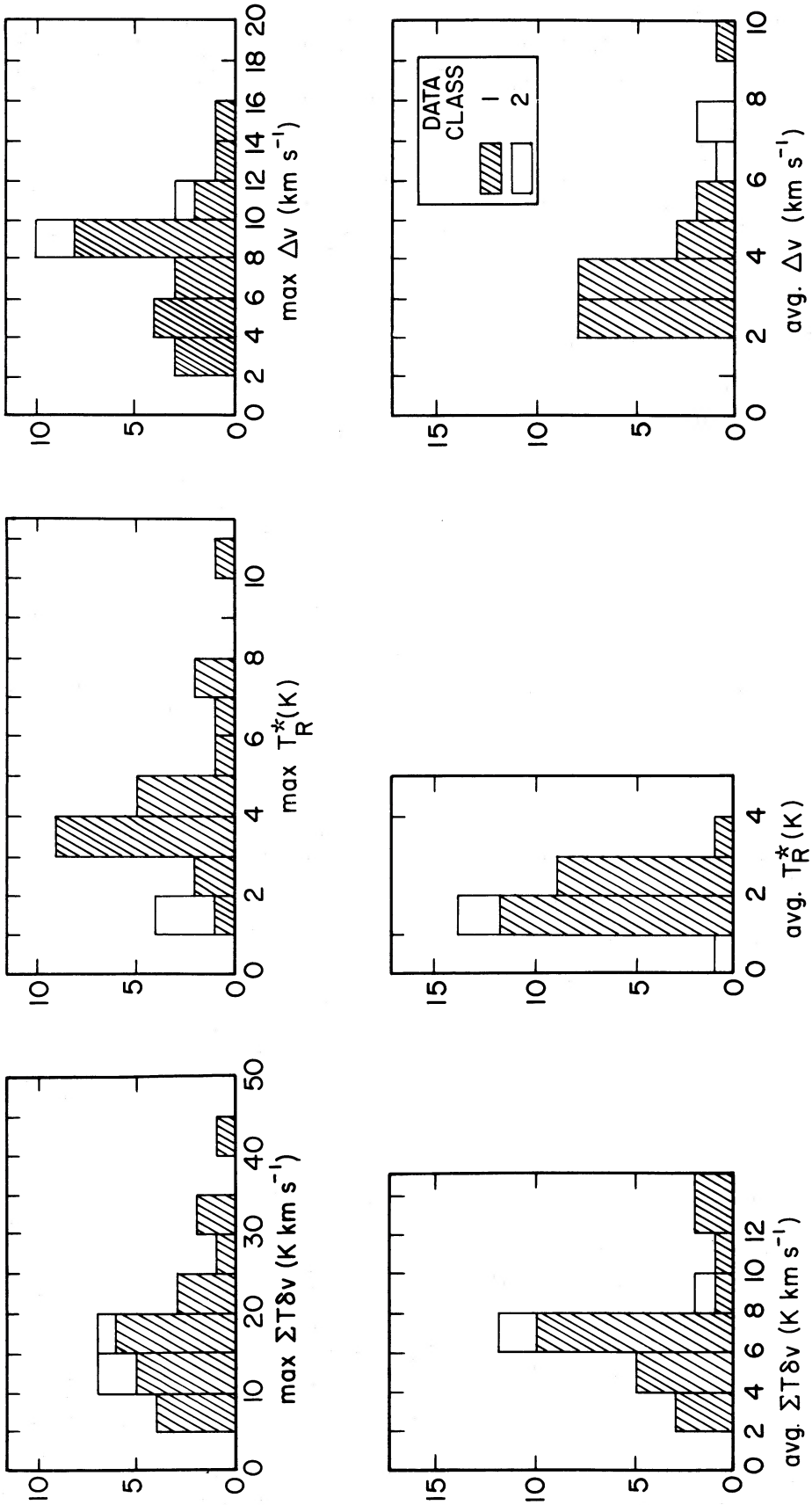

FIG. 4.—(*a*) Histograms of the maximum of the line parameters temperature, T_R^*, integrated intensity, $I = \Sigma T_R^* \delta v$, and linewidth, $\Delta v (= I/\text{peak } T_R^*)$, are shown. Each bin is segregated by data class (discussed in the text). KM clouds are not included in this figure. (*b*) An average of each line parameter, T_R^*, $\Sigma T_R^* \delta v$, and Δv was determined for each cloud. (All detected positions in a cloud were included in the average.) The resulting histogram for the ensemble of clouds is shown. Data bins are segregated by cloud data class (described in the text). KM clouds are not included in this figure.

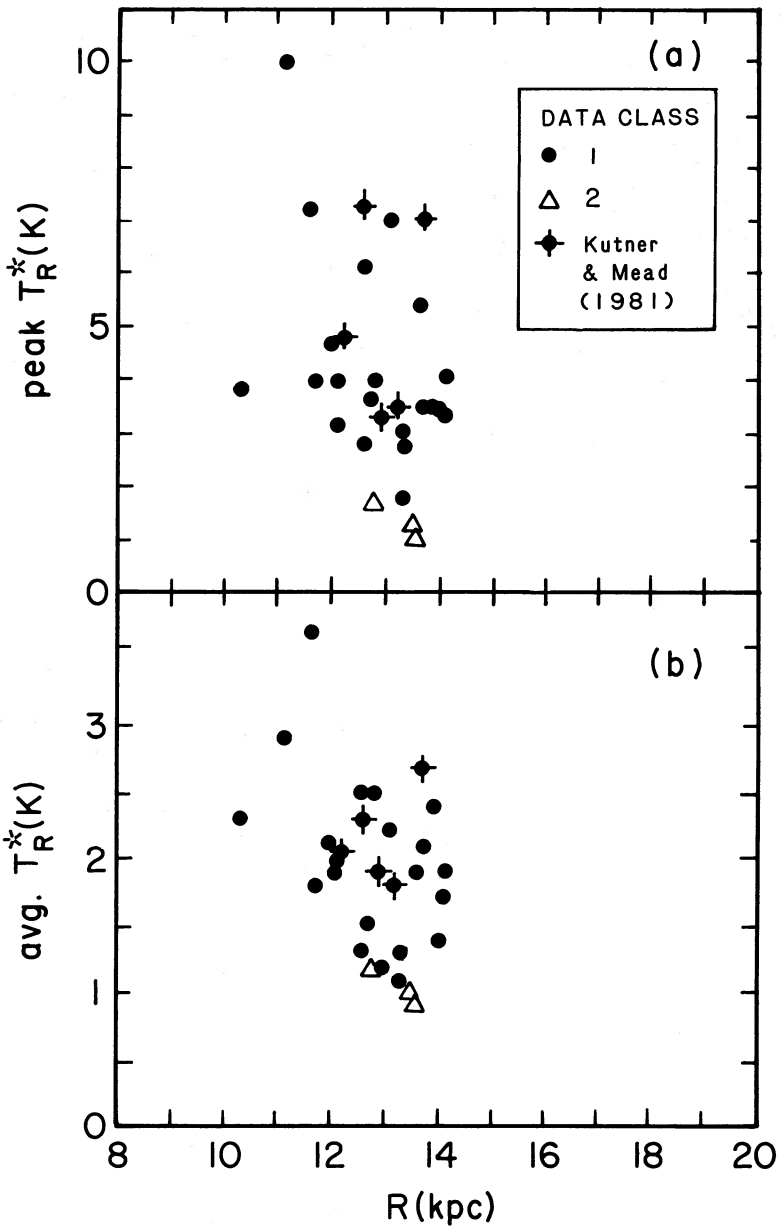

FIG. 5.—Peak and average line temperatures are plotted as a function of galactocentric distance, R. Each data class is represented by a different symbol. Clouds from KM are equivalent to data class 1 clouds but are plotted with separate symbols.

properly characterize the molecular material toward the edge of the Galaxy, a thorough, sensitive survey will be required, because of the low luminosity of the material.

In Figure 6 there is an indication of a gentle falloff in T_R^* with d. Since we do not expect a dramatic falloff of T_R^* in the range 5 kpc $< d <$ 15 kpc this plot is telling us that beam dilution is affecting our results at some level. Figure 5 shows essentially no decline of line strengths over the range of R where they are observed, indicating that any d effects seen in Figure 6 are independent of R effects.

The effect of beam size on line strength can be further examined by comparing $J = 2 \rightarrow 1$ and $1 \rightarrow 0$ line strengths (Table 1). Recall that the ^{12}CO ($J = 1 \rightarrow 0$) transition was observed with twice the beam size of the $J = 2 \rightarrow 1$ transition. So, if both lines are optically thick and thermalized (and the source fills both beams), the derived excitation temperatures should be equal. However, if the $J = 1 \rightarrow 0$ line is beam diluted, the $J = 2 \rightarrow 1$ line will be up to a factor of 4 times stronger because the beam is half the size. At positions where both transitions have been observed, the $J = 2 \rightarrow 1$ line is sometimes stronger by about 20% and sometimes weaker by about 30%; often the line strengths are the same, to within noise and calibration uncertainties. In one case, the $J = 2 \rightarrow 1$ line is twice as strong as the $1 \rightarrow 0$ line. We also observe some sources (e.g., G62.2+1.7) for which the $J = 2 \rightarrow 1$ line varies on a smaller scale than the $1 \rightarrow 0$ line, further indicating structure smaller than the $1 \rightarrow 0$ beam.

We conclude that peaks in the outer Galaxy clouds are

probably significantly beam diluted. Observations of these peaks with interferometer scale angular resolution is an obvious test of this hypothesis.

b) Physical Conditions

Next we investigate physical conditions (excitation temperature and optical depth) in the clouds. Qualitative analyses of the data and some quantitative results which can be derived directly from observations will be presented in the first four subsections. Results and analysis of models of cloud conditions (density, kinetic temperature, turbulent velocities and size scales, and relative abundances of ^{13}CO and ^{12}CO) will be presented in the subsequent subsections.

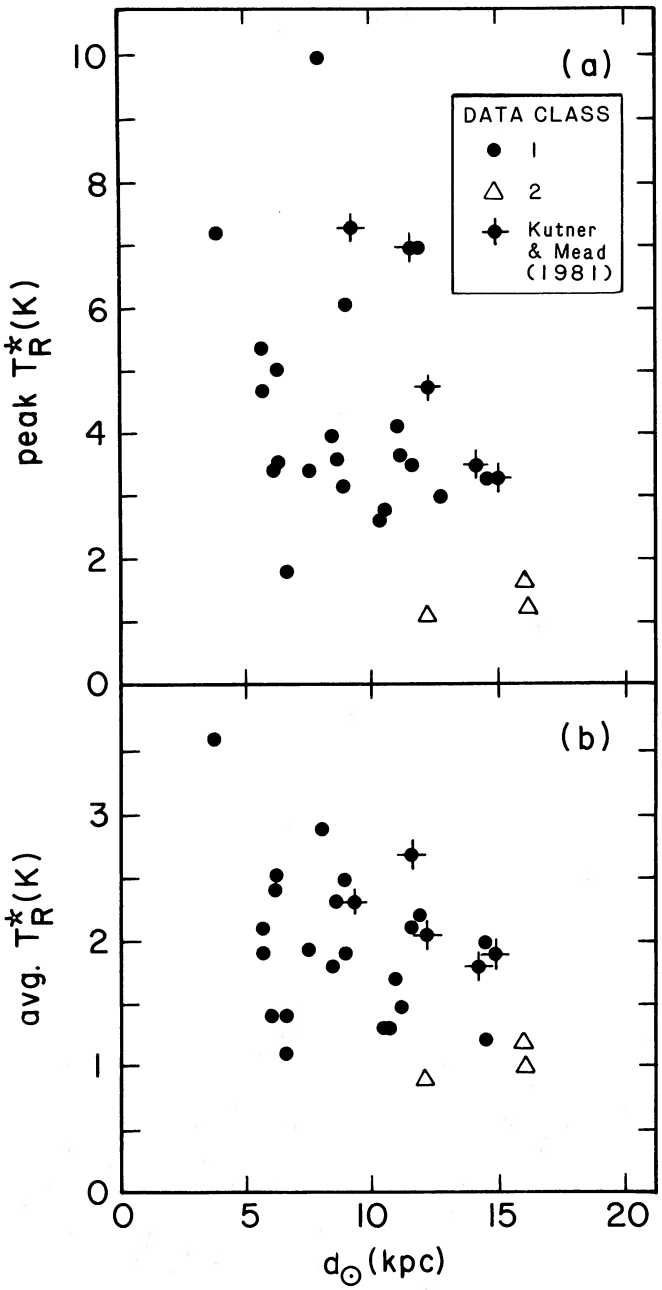

FIG. 6.—Peak and average line temperatures are plotted as a function of distance from the Sun, d. If the peaks are beam diluted there should be some correlation between T_R^* and d. Clouds from each data class and KM clouds (equivalent to data class 1) are represented by different symbols.

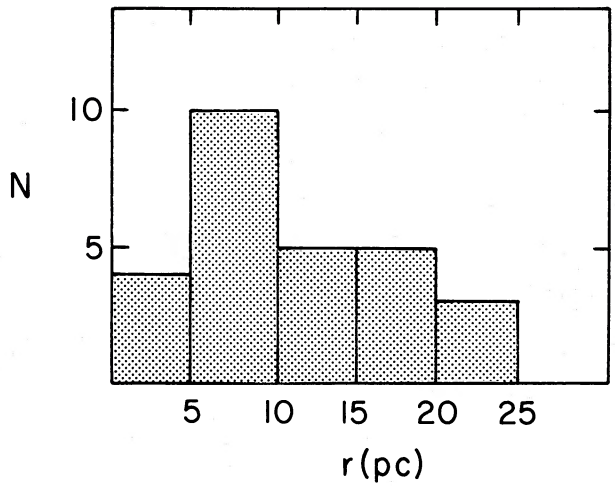

FIG. 7.—Cloud size distribution (derived from kinematic distances). The size, r, is the geometric mean of the semimajor and semiminor axes of a cloud: $r = (ab)^{0.5}$.

i) *Cloud Sizes*

Of the many results which will be derived from the data, the most straightforward is the cloud size. An effective radius, r, for each cloud was determined from the geometric mean of the semimajor and semiminor axes at the $T_R^* = 1$ K contour. If the outermost contour was greater than 1 K, the measurement was made to the most distant observed position. A histogram of cloud sizes is shown in Figure 7. If a typical GMC is 40 pc in the long dimension and 10 pc in the short dimension, then it has $r = 10$ pc. About half of our clouds are smaller and half larger than a typical ($r = 10$ pc) GMC. In at least three cases, the full extent of the cloud has not been mapped.

ii) *Excitation Temperatures*

Comparison of observational parameters of the three CO lines, CO ($J = 1 \rightarrow 0$), ^{13}CO ($J = 1 \rightarrow 0$), and CO ($J = 2 \rightarrow 1$), can yield information on the excitation and kinetic temperatures and the optical depth in a cloud. In the case of outer Galaxy clouds, this comparison is done to show that the low CO ($J = 1 \rightarrow 0$) T_R^*'s are not due to subthermal excitation of the line or low line optical depths. Once thermalization and optical thickness are established, line excitation temperatures and gas kinetic temperatures can be estimated.

Low radiation temperatures can be due to any of the following: (1) low optical depth, (2) low kinetic temperature, (3) subthermal excitation ($T_{ex} < T_k$) or (4) clumping. A line can be thermalized given sufficient optical depth, τ, or gas density, n, or an appropriate combination of τ and n. Observations of the ^{13}CO ($J = 1 \rightarrow 0$) and the CO($J = 2 \rightarrow 1$) line set limits on the optical depth and thermalization of the CO ($J = 1 \rightarrow 0$) line. At and near (within a few arcminutes of) outer Galaxy cloud peaks, typical $^{12}CO/^{13}CO$ ratios are 3 to 4, with a range of 2 to 10, indicating that the ^{12}CO ($J = 1 \rightarrow 0$) lines must be optically thick. The typical value of 3 to 4 is comparable to that for inner Galaxy clouds.

For an optically thick line, the excitation temperature can be derived from T_R^* via the expression

$$T_{ex} = \frac{h\nu/k}{\ln\{1 + h\nu/k/[(T_R^*/\eta_c) + T_{bg}]\}} \quad (1)$$

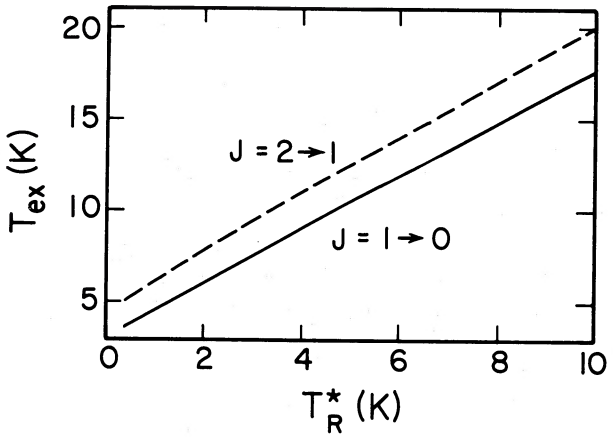

FIG. 8.—This plot shows the relationship between line temperature, T_R^*, and excitation temperature for the CO $J = 1 \rightarrow 0$ and $J = 2 \rightarrow 1$ lines assuming the source coupling efficiency, η_c, is 0.8 in each case.

where T_{bg} is the radiation temperature of the cosmic background and η_c is the source coupling efficiency. At a given frequency, ν, T_{bg} can be found from the expression,

$$T_{bg} = (h\nu/k)\{1/[\exp(h\nu/kT_B) - 1]\}, \quad (2)$$

where T_B is the temperature of the cosmic background, 2.7 K. For the $J = 1 \rightarrow 0$ and $2 \rightarrow 1$ lines, respectively, T_{bg} is 0.81 and 0.18 K. Figure 8 is a plot of T_{ex} versus T_R^* for the $J = 2 \rightarrow 1$ and $1 \rightarrow 0$ lines for our data (with η_c at both wavelengths equal to 0.8). It is often assumed that if both lines are thermalized and optically thick, their T_R's will be the same. However, Figure 8 shows that equal excitation temperatures result in slightly different T_R^*'s. For the low T_R^*'s in outer Galaxy clouds, this small difference can be an appreciable fraction of the line temperature.

We now consider whether equal excitation temperatures in the $J = 2 \rightarrow 1$ and $1 \rightarrow 0$ lines necessarily imply thermalization, thus allowing us to determine T_k directly from T_{ex}. Thermalization can be achieved at high gas densities, n, when collisions dominate in the excitation. However, in the presence of trapping of radiation, thermalization occurs at lower densities. When densities and optical depths are low, the collisional de-excitation rates for various transitions are comparable but the spontaneous decay rates are quite different, resulting in very different excitation temperatures in the transitions (see, e.g., Leung 1975). Thus, unless the transitions are thermalized (de-excitation also dominated by collisions), the excitation temperatures for the two transitions will be different. In § IV*b*iii, models will be presented which account for trapping and we will show that these lines are thermalized. We can confidently assume that these lines are optically thick and thermalized.

A comparison of outer and inner Galaxy cloud kinetic temperatures would be illuminating. However, in the case of the peaks this is difficult because they are beam diluted by an unknown amount. Comparing temperatures in cloud envelopes involves a different set of considerations from peak temperature comparisons. Unless the clump filling factor for outer Galaxy clouds is less than that for inner Galaxy clouds, beam dilution should not affect a comparison of envelope temperatures. Kutner and Leung (1985) chose a kinetic temperature of 13 K for their models of nearby dark globules and GMCs in the molecular ring. Most outer Galaxy clouds have average line temperatures, T_R^*'s, [CO($J = 1 \rightarrow 0$)] of 2–3 K (Fig. 4), indicating kinetic temperatures of no more than 8 K. This average includes all psotions out to the $T_R^* = 1$ K contour. If envelope is defined as some intermediate (in T_R^*) region of the cloud, not including peak or 1 K positions, then the average T_R^* will be at most 5 K for a given cloud. A 5 K T_R^* implies a T_k of 10 K (again assuming the necessary assumptions are valid). So, the outer galaxy clouds appear to be about a factor of 1.5 times (8 versus 13) cooler than inner galaxy clouds.

iii) *Model Results*

Because of the complicated physics in clouds, we have used computer models to determine a quantitative range of probable physical conditions in the clouds. C. M. Leung has kindly provided us with results from his code which solves the multilevel, non–LTE line transfer problem using the quasi-diffusion method (Leung 1975). This is the same model used in Kutner and Leung (1985), discussed below.

Our goal was to model the envelopes of the clouds to (1) confirm our assertion that the observed envelope line intensities can be explained by lower kinetic temperatures in the outer Galaxy clouds compared to inner Galaxy GMCs with massive-star formation and (2) quantitatively determine the H_2 density and CO abundance. Rather than model a specific cloud, our interest was in determining a range of model parameters which match the range of observed parameters. Cloud peaks were not modeled because the extent to which beam dilution has affected our results is unknown. Furthermore, internal heat sources and their effect on the surrounding cloud are more difficult to model, especially when few observational details are available to guide the choice of input parameters. So, a cloud with uniform density and temperature was assumed.

Since our interest was in finding a range of models which matched typical observed parameters, we defined a generic cloud and matched the model results to it. The generic cloud is essentially the average of all observed clouds. For each cloud observed in both CO lines, an average T_R was determined for each line over the region observed in both lines. The few strongest positions were not included in the average. These averages were then averaged to find $T_R(1 \rightarrow 0)$ and $T_R(2 \rightarrow 1)$ for the generic cloud. Table 2 contains the information used to determine the T_R's of the generic cloud; for the $J = 1 \rightarrow 0$ and $2 \rightarrow 1$ line respectively, $T_R = 3.0$ and 2.0 K. From cloud averages and inspection of the spectra maps, a ^{13}CO T_R^* of ~ 0.7 K was determined to be appropriate for comparison.

Input parameters were chosen to cover a range of possible conditions. In local GMC envelopes, the H_2 density, n is typically 300 particles per cm^{-3}, and for extended local dark clouds, typical densities are about 1000 particles per cm^{-3}; so all models were run at both of these densities. Models were run for three different values of the CO to H_2 abundance, X(CO): 1, 5, and 20×10^{-5}. The intermediate X(CO) is a rough average of what most authors use for GMCs, as discussed by Kutner and Leung (1985). Temperatures were chosen from estimates derived from observational results. The derivation of cloud kinetic temperatures from observed line strengths was discussed in the previous section. This was done for the "generic" cloud and the result, 7 K, was chosen as the lowest input T_k. Other input temperatures were chosen to be 10 and 13 K, the latter being typical of molecular ring and local GMC envelopes. Clouds were modeled with radii, R, of 2, 5, and 10

pc. The product $2n\,RX$ is equal to the column density, so for a given X and n, varying R varies the column density and the dependence of line strength on column density can be seen. The parameter ranges (n, T_k, and X) were chosen based on the knowledge that CO line strength depends sensitively on kinetic temperature and less sensitively on the density and CO abundance (Kutner and Leung 1985).

Model T_R's ($\equiv T_R^*/\eta_c$) for the CO $J = 1 \rightarrow 0$ and $2 \rightarrow 1$ lines were compared to generic cloud T_R's. As a final test for the appropriate model, ^{13}CO T_R's were compared. These data are not as good as the CO data and were used to eliminate models which had matching CO data but which had ^{13}CO lines which were too strong.

A tabulation of all the model results is presented in Table 3. All 10 and 13 K models, except those with $X = 1 \times 10^{-5}$ and $n = 300$ cm^{-3}, can immediately be ruled out because the line

TABLE 3

MODEL RESULTS

				T_R		
T_k (K)	[CO]/[H$_2$] ([^{13}CO]/[H$_2$])	n (cm^{-3})	r (pc)	CO (J = 1–0) (K)	CO (J = 2–1) (K)	^{13}CO (J = 1–0) (K)
7.....	1×10^{-5}	1000	2	3.0	1.7	0.65
	(2×10^{-7})		5	3.3	1.9	...
			10	3.4	2.0	1.1
		300	2	1.4	0.38	0.1
			5	1.7	0.50	0.15
			10	2.1	0.71	...
	5×10^{-5}	1000	2	3.5	2.3	1.7
	(1×10^{-6})		5	3.5	2.5	2.0
			10	3.6	2.5	2.2
		300	2	2.8	1.2	0.36
			5	2.9	1.3	0.49
			10	3.0	1.6	0.61
	2×10^{-4}	1000	2	3.7	2.5	2.7
	(4×10^{-6})		5	3.7	2.5	2.9
			10	3.7	2.5	3.0
		300	2	3.2	2.1	0.83
			5	3.5	2.2	1.10
			10	3.5	2.3	1.34
10.....	1×10^{-5}	1000	2	5.4	3.3	1.0
	(2×10^{-7})		5	5.5	3.9	1.5
			10	5.8	4.1	1.8
		300	2	2.4	0.8	...
			5	3.0	1.1	...
			10	3.3	1.5	...
	5×10^{-5}	1000	2	6.1	4.3	2.9
	(1×10^{-6})		5	6.2	4.8	3.4
			10	6.2	5.0	3.8
		300	2	4.5	2.4	...
			5	5.1	2.8	...
			10	5.3	3.1	1.1
	2×10^{-4}	1000	2	6.5	5.0	4.5
	(4×10^{-6})		5	6.6	5.0	5.0
			10	6.6	5.1	5.3
		300	2	5.5	4.1	1.4
			5	5.6	4.5	1.7
			10	...	...	...
13.....	1×10^{-5}	1000	2	7.1	4.6	1.2
	(2×10^{-7})		5	7.5	5.5	1.7
			10	7.7	6.0	2.2
		300	2	2.8	1.1	...
			5	3.5	1.4	0.3
			10	4.2	1.9	0.4
	5×10^{-5}	1000	2	8.6	6.4	3.5
	(1×10^{-6})		5	8.8	7.0	4.3
			10	8.9	7.4	4.9
		300	2	5.5	3.3	0.8
			5	6.5	3.9	1.0
			10	...	...	1.3
	2×10^{-4}	1000	2	9.0	7.6	...
	(4×10^{-6})		5	9.4	7.8	...
			10	9.6	7.7	...
		300	2	7.5	5.7	...
			5	...	...	...
			10	...	...	...

strengths are too large. At 7 K, the $n = 1000$ cm^{-3}, $X = 5 \times 10^{-5}$ and 20×10^{-5} models can be ruled out because the ^{13}CO lines are too strong. Also at 7 K, the $n = 300$ $Q = 1 \times 10^{-5}$ model does not match the generic cloud because the lines are too weak. (This model may be appropriate for positions near a cloud edge, defined by the $T_R^*(J = 1 \rightarrow 0) = 1$ K contour, but there is insufficient $2 \rightarrow 1$ and ^{13}CO data at those positions to be sure.)

Of the five possible models that remain the ones at 10 K and at 13 K, both with $n = 300$ cm^{-3} and $X = 10^{-5}$, can be eliminated via the following argument. For our generic cloud the T_{ex}'s derived from the T_R^*'s of the two lines are essentially the same (see Fig. 9), so a realistic model must also produce lines which have equal (or nearly so) excitation temperatures. For the two models in question, the T_{ex}'s of the two lines are very different, so we can reject these two higher temperature, low n and low Q models. An additional problem with the 13 K model is that ratio $T_R(^{12}\text{CO})/T_R(^{13}\text{CO})$ is more than 10 while we have set 6 as the highest acceptable ratio.

Probable cloud models are as follows, $T_k = 7$ K with (1) $X = 10^{-5}$ and $n = 1000$ cm^{-3}, (2) $X = 5 \times 10^{-5}$ and $n = 300$ cm^{-3}, (3) $X = 2 \times 10^{-4}$ and $n = 300$ cm^{-3}. *At 7 K there is a range of parameters which produce the observed range of line temperatures; this is not true for the higher temperature models.* That all possible models are at 7 K confirms our contention that the clouds have low kinetic temperatures and therefore, that low line temperatures are the result of inherently low cloud temperatures rather than subthermal excitation.

iv) *Mass Derivation*

1. CO *masses.*—Cloud masses have been determined by converting ^{12}CO integrated intensities to molecular hydrogen abundances. Kutner and Leung (1985) have studied the conversion of CO integrated intensities to molecular hydrogen abundances. The multilevel, non–LTE line transfer problem was solved using the quasi-diffusion method (Leung 1975) for a cloud model with a given density and temperature distribution. They found that ^{12}CO integrated intensities are related to molecular hydrogen column densities and that the ratio varies with kinetic temperature: $I_{12}/N_{H_2} \sim T_k^{1.33}$. In addition, they found that at low ($T_k \sim 6$ K) temperatures the ^{13}CO LTE column density underestimates the true column density by a factor of up to 10. For this reason we have used the I_{12} conversion method here rather than the $N13$ (LTE) method. The proportionality of I to N holds *only* if the cloud turbulent velocity increases with cloud size. The relation $v_{turb} \propto r^{0.5}$ has been determined empirically by Leung, Kutner, and Mead (1982) for globules and by Dame *et al.* (1986) for GMCs and is the relation used by Kutner and Leung (1985).

We have used our cloud sample to see if a similar result holds for outer Galaxy clouds. The result is shown in Figure 9, log (Δv) versus log (r) is plotted. In this case, Δv is I_{12}/T_{12} at the peak, and r is the geometric mean of the long and short axes. There is clearly a correlation, and a least squares fit to a straight line gives $\Delta v \propto r^{0.4}$. Considering the uncertainties, it appears that the line width–cloud size relationship for outer Galaxy clouds is comparable to that in inner Galaxy GMCs and globules. Therefore, the $I12$ method should yield reliable mass estimates of outer Galaxy clouds.

We have used the conversion factor, $N_{H_2}/I12 = 4 \times 10^{20}$ cm^{-2}(K km s^{-1})$^{-1}$ in our calculations. This is twice what Dame *et al.* (1986) used for the inner Galaxy; other authors (e.g., Solomon, Scoville, and Sanders 1979) have used 4×10^{20} for the inner Galaxy. Kutner and Leung claim that 2×10^{20} is the appropriate number for the inner Galaxy because the CO is generally warmer (T_k is larger) in the inner Galaxy. In other words, at a given H_2 column density, CO integrated intensities will be higher in the inner Galaxy than in the outer Galaxy because the outer Galaxy is cooler.

Since many of the maps were not fully sampled, especially in the envelopes, calculated masses were scaled up to account for this. For each cloud an estimate of the proportion of unmapped to mapped positions, weighted by the integrated intensity, was made from a visual inspection of the map. No extrapolation was made about the extent of the cloud; only positions contained in a boundary of mapped positions with lines were considered. The "percent mapped" column in Table 4 indicates our estimate of the fraction of the mass we have actually mapped. The masses in Table 4 have already been scaled up for this effect.

2. *Virial masses.*—We have used our data to calculate virial masses, as a check on the CO masses. The virial mass, M_{VT}, is determined from the expression,

$$M_{VT} = (363\ M_\odot)(r/1\ \text{pc})(\Delta v/1\ \text{km s}^{-1})^2\ ,$$

where r is the cloud radius (§ IV*bi*) and Δv is the line width determined from a composite spectrum for each cloud. If we assume clouds of uniform density, the numerical coefficient would be 208 instead of 363. We have chosen the larger number, corresponding to a $1/r$ density distribution, to be consistent with the studies of inner Galaxy cloud properties by Solomon *et al.* (1987).

In Figure 10, we compare the virial masses with the CO masses and CO luminosities. The CO luminosity is a good basis for comparison of inner and outer Galaxy clouds, since it does not involve any assumptions about $N_{H_2}/I12$. The two quantities are related by $(M_{CO}/M_\odot) = (1.59)a(I_{CO}/1\ \text{K km s}^{-1}$ pc), where $a = (N_{H_2}/10^{20}\ \text{cm}^{-2})/I12$. (In our case, $a = 4$.)

From Figure 10 we see that there is a good correlation between M_{VT} and L_{CO}. A least squares fit to a straight line on the log-log plot (ignoring one cloud, G75, which appears to have unusually broad lines), gives

$$(M_{VT}/M_\odot) = (78)(L_{CO})^{0.76 \pm 0.08}.$$

For comparison, Solomon *et al.* (1987) found a similar expression for inner Galaxy clouds, with essentially the same power, 0.81 ± 0.03, and a coefficient of 39, instead of our 78. The

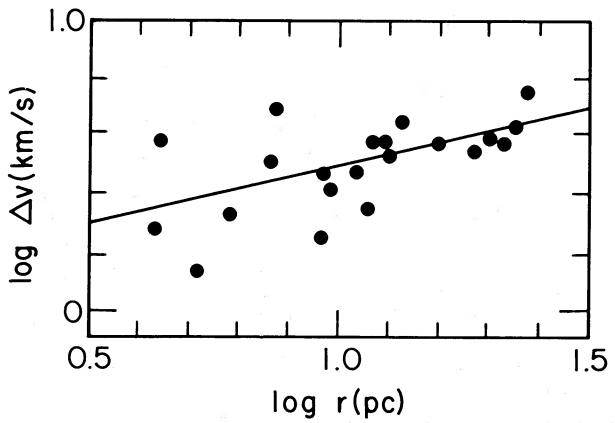

FIG. 9.—Line width–cloud size relationship. Δv is $I12/T12$ at the peak, and r is the geometric mean of the semimajor and semiminor axes.

TABLE 4

CLOUD MASSES

Name	Percent Mapped	M_{CO} ($10^4 M_\odot$)	M_{vt} ($10^4 M_\odot$)
G56.8+1.9	65	14.0	14.6
G59.9+1.5[a]	100	5.8	7.7
G62.2+1.7	90	0.5	1.3
G65.5+1.3[a]	100	6.8	13.8
G69.7+1.5[a]	100	10.0	12.0
G74.1+1.5	<30	4.0	3.1
G75.0+1.9	60	1.5	17.0
G78.8+1.7	90	7.0	9.4
G80.1+1.9	100	2.0	8.4
G83.3+1.9	60	2.0	1.7
G84.7+1.7[a,b]	100	18.0	24.4
G85.0+2.4[c]	65	2.0	2.1
G85.0+2.4[d]	80	3.0	4.0
G88.4+1.9[e]	<50	2.0	3.3
G88.4+1.9[f]	90	0.6	0.9
G88.8+1.9	<50	1.2	1.6
G89.9+1.3[a]	100	6.3	5.7
G92.9+1.9	90	2.0	5.7
G93.2+1.7	100	2.0	2.6
G115.2+2.0	95	0.5	1.2
G120.8+1.1	50	11.0	25.6
G123.5+2.0	<25	1.1	11.8
G124.4+2.0	65	4.0	5.4
G140.5+0.5	<50	0.9	2.3
G211.4−1.1	80	0.5	1.3
G212.1−1.1	<60	0.5	4.2
G215.0+0.9	<30	4.0	3.1

[a] KM cloud.

[b] This cloud is mapped incompletely under the name G84.7+1.9.

[c] −51 km s^{-1} cloud.

[d] −83 km s^{-1} cloud.

[e] −64 km s^{-1} cloud.

[f] −79 km s^{-1} cloud.

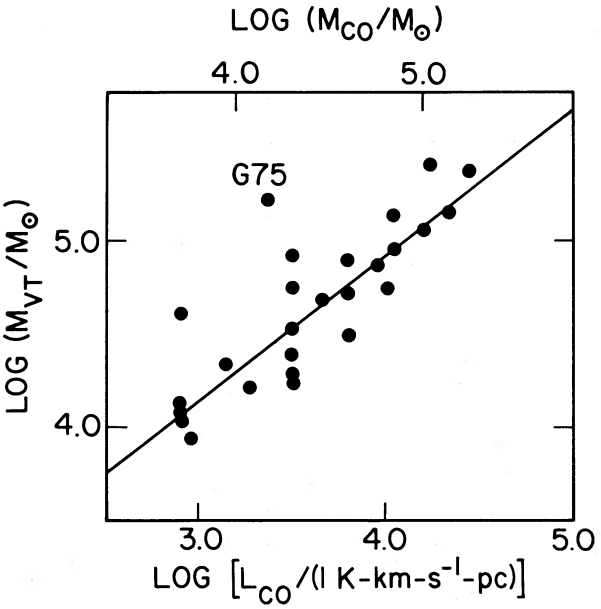

FIG. 10.—Virial mass as a function of CO luminosity. On the upper axis are the masses corresponding to the luminosities on the lower axis, on the assumption that $N_{H_2}/I12 = 4 \times 10^{20}$ cm^{-2} (K km s^{-1})$^{-1}$. The straight line is a least squares fit to the data (excluding G75, a small cloud with unusually broad lines).

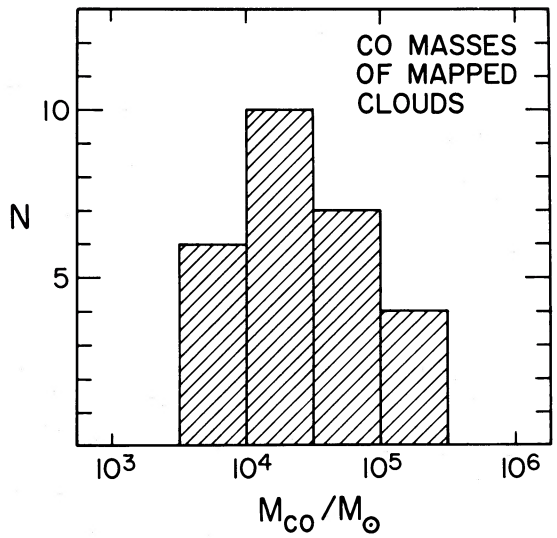

FIG. 11.—A histogram of logarithm of cloud mass is shown.

agreement of the power laws suggests that the variation of $N_{H_2}/I12$ with cloud mass is the same for inner and outer Galaxy clouds. However, the factor of 2 larger coefficient for the outer Galaxy clouds means that they are, *per unit virial mass, a factor of 2 less luminous in CO emission* than their inner Galaxy counterparts. This is independent confirmation of the idea, discussed above, that for outer Galaxy clouds, we must use a value of $N_{H_2}/I12$ which is a factor of 2 larger than for inner Galaxy clouds.

3. *Cloud mass distribution.*—Figure 11 is a histogram of number of clouds versus log M. The masses of many of the outer galaxy clouds are comparable to those of inner galaxy GMCs, while, as a group, outer galaxy clouds are roughly 10 times less massive than the biggest well-studied clouds of 10^6 $M_\odot$. It is tempting to draw the additional conclusion that, like the inner Galaxy, most of the molecular mass in the outer Galaxy is in a few massive clouds rather than a large number of small clouds. However, because our initial survey was undersampled and because of the subjective way the individual clouds were chosen, the smaller cloud part of the distribution is undetermined at this time. To obtain an unbiased cloud size distribution, a section of the outer Galaxy must be fully sampled with good sensitivity and good angular resolution. Last, we would like to recommend caution when comparing such things as mass and size distributions because some authors' "clouds" are other authors' "cloud complexes," with each complex containing several clouds. (For example, Myers *et al.* (1986), in their study of the inner Galaxy, have a much coarser scale of study than in this work because of the large beam used for their CO [8′] and infrared [*IRAS* at 100 μm is 4′] observations. Structures which they call clouds would be called complexes in the context of this work.)

v) *Cosmic-Ray Heating*

In § IV*b*ii possible causes were discussed for the low antenna temperatures in outer Galaxy clouds. If the clouds have low kinetic temperatures, then one would like to know why. A thorough analysis of the thermal balance in the clouds must be deterred until more data are available, but a preliminary excursion into this area is of interest. Various processes can heat the

envelopes of molecular clouds. In outer Galaxy clouds the two most important are probably cosmic rays and, via the dust, H II regions. At some distance from the internal heat source the two processes will supply equal amounts of heat to the cloud. It may be that the H II region energy is efficiently transported to large distances, making cosmic-ray heating relatively unimportant. But it is likely that cosmic rays are the dominant heat source for some fraction of the cloud.

It has been suggested that there is a (galactocentric) radial gradient in the cosmic-ray flux. Less heating by cosmic rays could result in lower kinetic temperatures in the envelopes of the outer Galaxy clouds. How much would the cosmic-ray flux have to drop in order to cause the observed contrast between antenna temperatures in the inner and outer Galaxy?

The cosmic-ray heating rate in dense clouds is (Goldsmith and Langer 1978)

$$\Gamma_{\rm cr} = \zeta_p(\mathrm{H}_2)\Delta Q_{\rm cr}\, n(\mathrm{H}_2)\,, \tag{3}$$

where ζ_p is the direct (primary) cosmic-ray ionization rate of H_2 and $\Delta Q_{\rm cr}$ is the energy deposited as heat as a result of an ionization. Estimates of the ionization rate, ζ_p, range from (3–30) $\times 10^{-18}$ s^{-1} (see Goldsmith and Langer [1978] and references therein). For 10 MeV protons, $\Delta Q_{\rm cr} \sim 17$ eV and for 100 MeV protons, $\Delta Q_{\rm cr} \sim 26$ eV.

To see how the cosmic-ray heating rate affects the gas kinetic temperature we again follow Goldsmith and Langer. At very low temperatures (~ 10 K), the cooling rate is

$$\Lambda = n(\mathrm{H}_2)a \exp(-T_e/T)\,, \tag{4}$$

where T_e is the characteristic effective level spacing for CO and a is a constant. For the $J = 1 \rightarrow 0$ transition the characteristic temperature is 5.6 K and $T_e \sim 10$–25 K for CO in general. In equilibrium, the cooling and heating rates are equal and we can solve for the temperature. We can compare inner and outer Galaxy temperatures as a function of inner and outer Galaxy cosmic-ray heating rates by taking the ratio of Γ(inner) to Γ(outer) and solving for T,

$$T_{\rm inner} - T_{\rm outer} = -T_e \ln(\Gamma_{\rm outer}/\Gamma_{\rm inner})\,. \tag{5}$$

A factor of 10 decrease in heating rate yields a difference in temperature of 23 K for an effective spacing, T_e, of 10 K. A factor 2 decrease in heating rate yields a temperature difference of 7 K with the same T_e. Temperature differences are proportional to T_e. Therefore, a drop in cosmic-ray heating could cause a drop in gas temperatures from the inner to the outer Galaxy.

However, the heating rate depends on the *number* of cosmic rays and on their energy *spectrum*. Bhat *et al.* (1985) and Bloeman *et al.* (1986) have shown that the cosmic-ray number intensity (units of [cm^2 s sr]$^{-1}$ or [H atom s sr]$^{-1}$) is lower in the outer Galaxy. They also show that the number intensity of lower energy (70–150 MeV) cosmic rays drops more precipitously than the intensity of higher energy (150 MeV–5 GeV) cosmic rays. If the higher energy cosmic rays pass through outer Galaxy clouds, then, because there are fewer lower energy cosmic rays, the cosmic-ray heating rate will be lower in the outer Galaxy.

V. SUMMARY

We have mapped CO ($J = 1 \rightarrow 0$) emission from 31 molecular clouds in the outer Galaxy. The CO ($J = 2 \rightarrow 1$) and ^{13}CO ($J = 1 \rightarrow 0$) lines have each been observed from 11 and 10 clouds, respectively.

1. The clouds follow the H I warp, and there is evidence for an armlike concentration at $R \approx 13$ kpc in the first quadrant.

2. Beyond $R \sim 14$ kpc, only weak lines are observed. This may indicate that the edge of the Galaxy, in terms of molecular material, is around $R = 14$ kpc. On the other hand, the material beyond that may be very cold, rather than sparse.

3. Normal CO optical depths in the vicinity of the peaks of the clouds are indicated by $T_R^*(\mathrm{CO})/T_R^*(^{13}\mathrm{CO})$ ratios ranging from 3 to 6.

4. Peak line strengths are considerably less than those found in inner Galaxy GMC cores. Beam dilution may account for the difference between outer Galaxy peaks and typical inner Galaxy peaks.

5. Cloud dimensions are typical of inner Galaxy GMCs, the average radius being 11.5 pc (where r is the geometric mean of the semimajor and semiminor axes of the cloud).

6. Cloud envelopes are less luminous than in typical inner Galaxy GMCs. Comparison of the excitation temperatures of the $1 \rightarrow 0$ and $2 \rightarrow 1$ transitions of CO indicate that the lines are thermalized, and typical cloud kinetic temperatures are 7 K.

7. To properly account for radiative transfer effects in the clouds, models were run for uniform temperature and density clouds. Models run with higher T_k (10 and 13 K) produced line strengths larger than observed line strengths. The data can be fitted by a range of models with $T_k = 7$ K. The densities and abundances in these models are characteristic of inner Galaxy GMCs.

8. We estimate that a factor of 2 decrease in the cosmic-ray heating rate would result in a 7 K difference in cloud kinetic temperature. If the cosmic-ray heating rate does drop with R, this could explain the lower temperatures of outer galaxy clouds.

9. Most observed clouds have masses between 10^4 and $10^5\,M_\odot$.

Outer Galaxy molecular clouds appear to have some properties in common with local dark clouds and some in common with inner galaxy GMCs (though demarcations between these and other cloud types are admittedly ill-defined). Like GMCs, outer Galaxy molecular clouds form O and B stars (as discussed in Papers I and IV), but their envelope temperatures are closer to those of dark clouds. While the outer Galaxy cloud masses are clearly greater than those of dark clouds, the upper end of the mass range does not extend as high as the upper end of the mass range for inner Galaxy GMCs (up to $\sim 10^6\,M_\odot$). Apparently, outer Galaxy molecular clouds represent a distinct cloud category, in some ways intermediate between dark clouds and inner Galaxy GMCs. If this turns out to be the case, it is most likely the result of the different environments in the inner and outer Galaxy.

This work presents the basics of the nature and distribution of outer Galaxy molecular clouds and provides the background for further study of galactic structure, star formation, and molecular clouds. A reliable rotation curve and the lack of distance ambiguities make these studies much simpler in the outer Galaxy than in the inner Galaxy.

Determination of the large-scale characteristics of the outer Galaxy is hampered by the lack of a survey with extensive (l, b) coverage, thorough sampling, and high sensitivity such as those available of the inner Galaxy. From such a set of data, a more accurate determination could be made of the mass and

(R, z) distribution of the molecular material in the outer Galaxy. In particular, because the armlike feature at 13 kpc is well defined, comparison of arm and interarm cloud populations will be easier than in the inner Galaxy where the demarcations between arms and interarms are less clear. With a limited (in l) but fully sampled survey, cloud size distributions could be obtained. Groups of spectra could be obtained which reveal "slices" through complete arm and interarm regions. A related study could focus on the cool clouds beyond $R = 14$ kpc. These clouds may be at (or near) the molecular edge of the Galaxy and therefore interesting in their own right.

Studies of individual clouds are at the stage of inner Galaxy clouds a decade or two ago. We know that there are H II regions associated with the larger outer Galaxy clouds but further study of cloud physical conditions with molecules such as NH_3, H_2CO, CS, etc., is still to be done. Molecular outflows, so ubiquitous in inner Galaxy and local clouds (whether they are forming massive stars or not), have not yet been searched for in the outer Galaxy. Detailed study of the cloud peaks will require interferometric observations because of the large distances to the clouds. Understanding outer Galaxy clouds will lead to an understanding of the effects of, for example, cosmic rays and spiral arm passages on molecular clouds and star formation.

This work was supported by NSF grant AST81-20500, and a gift from an anonymous donor to support student research in astrophysics at RPI. We would also like to thank C. M. Leung for kindly providing us with the results of radiative transfer models. We would like to thank the referee for a thoughtful and thorough reading of the manuscript. Part of this work was taken from a thesis submitted in partial fulfillment of the requirements for the Ph.D. degree in the Department of Physics of Rensselaer Polytechnic Institute.

REFERENCES

Bhat, C. L., Issa, M. R., Houston, B. P., Mayer, C. J., and Wolfendale, A. W. 1985, *Nature*, **314**, 511.
Bloemen, J. B. G. M., *et al.* 1986, *Astr. Ap.*, **154**, 25.
Brandt, J. 1986, Ph.D. thesis, Leiden University.
Burton, W. B. 1972, *Astr. Ap.*, **19**, 51.
Clemens, D. P., Sanders, D., Scoville, N. Z., and Solomon, P. M. 1986, *Ap. J. Suppl.*, **60**, 297.
Cohen, R. S., and Thaddeus, P. 1977, *Ap. J.* (*Letters*), **217**, L155.
Dame, T. M. 1984, Ph.D. thesis, Columbia University.
Dame, T. M., Elmegreen, B. G., Cohen, R. S., and Thaddeus, P. 1986, *Ap. J.*, **305**, 892.
Goldsmith, P. F., and Langer, W. D. 1978, *Ap. J.*, **222**, 881.
Henderson, A. P., Jackson, P. D., and Kerr, F. D. 1982, *Ap. J.*, **263**, 116.
Kulkarni, S. R., Blitz, L., and Heiles, C. 1982, *Ap. J.* (*Letters*), **259**, L63.
Kutner, M. L. 1978, *Ap. Letters*, **19**, 81.
———. 1983, in *Surveys of the Southern Galaxy*, ed. W. B. Burton and F. P. Israel (Dordrecht: Reidel), p. 143.
———. 1984, *Fund. Cosmic Phys.*, **9**, 233.
———. 1986, in *IAU Symposium 115, Star Forming Regions*, ed. M. Peimbert (Dordrecht: Reidel), in press.
Kutner, M. L., and Leung, C. M. 1985, *Ap. J.*, **291**, 188.
Kutner, M. L., and Mead, K. N. 1981, *Ap. J.* (*Letters*), **249**, L15 (KM).
Kutner, M. L., and Mead, K. N. 1985, in *IAU Symposium 106, The Milky Way Galaxy*, ed. H. van Woerden, W. B. Burton, and K. J. Allen (Dordrecht: Reidel), p. 209.
Kutner, M. L., Mundy, L., and Howard, R. 1984, *Ap. J.*, **283**, 890.
Kutner, M. L., and Ulich, B. L. 1981, *Ap. J.*, **250**, 341.
Leung, C. M. 1975, Ph.D. thesis, University of California, Berkeley.
Leung, C. M., Kutner, M. L., and Mead, K. N. 1982, *Ap. J.*, **262**, 583.
Mead, K. N. 1986*a*, *Bull. AAS*, **117**, 870.
———. 1986*b*, Ph.D. thesis, Rensselaer Polytechnic Institute.
———. 1988, submitted to *Ap. J.*, Paper II.
Mead, K. N., Kutner, M. L., and Evans, N. J., II 1988, in preparation, Paper IV.
Mead, K. N., Kutner, M. L., Evans, N. J., II, Harvey, P. M., and Wilking, B. A. 1987, *Ap. J.*, **312**, 321 (Paper I).
Myers, P. C., Dame, T. M., Thaddeus, P., Cohen, R. S., Silverberg, R. F., Dwek, E., and Hauser, M. G. 1986, *Ap. J.*, **301**, 398.
Solomon, P. M., Rivolo, A. R., Barrett, J., and Yahil, A. 1987, *Ap. J.*, **319**, 730.
Solomon, P. M., Scoville, N. Z., and Sanders, D. 1977, *Bull. AAS*, **9**, 554.
Solomon, P. M., Stark, A. A., and Sanders, D. B. 1983, *Ap. J.* (*Letters*), **267**, L29.
Weaver, H., and Williams, D. R. W., 1973, *Astr. Ap. Suppl.*, **17**, 1.
Wright, A. E., and Barlow, M. J. 1975, *M.N.R.A.S.*, **170**, 41.

MARC L. KUTNER: Department of Physics, Rensselaer Polytechnic Institute, Troy, NY 12180-3590

KATHRYN N. MEAD: Code 4138ME, Naval Research Laboratory, Washington, DC 20375-5000